To be published in Applied Optics:

Title: On the determination of optical properties for thin metallic films
Authors: Jeremy Orosco,Carlos Coimbra
Accepted: 30 May 18
Posted 01 June 18
Doc. ID: 325175

On a causal dispersion model for the optical properties of thin metallic films

J. Orosco[1] and C. F. M. Coimbra[1,*]

[1] Department of Mechanical and Aerospace Engineering, Center for Energy Research, University of California San Diego, La Jolla, CA 92093-0411
[*] Corresponding author: ccoimbra@ucsd.edu

Compiled May 22, 2018

A causal model that is fully compliant with the Kramers-Kronig Relations (KKRs) is used for characterizing the optical response of metals exhibiting sharp, non-Lorentzian regions of interband absorption. This consistent model also recovers the Gaussian character of the broadened peaks observed in the infrared response of amorphous materials. A reductive procedure for optimal fitting of KKR-compliant composite models to the permittivity data of metals over the intraband and interband energetic regimes is introduced and applied to eleven metals: Ag, Au, Cu, Al, Be, Cr, Ni, Pd, Pt, Ti, and W. We show that results obtained using this optimal procedure outperform—both qualitatively and quantitatively—those obtained by previous non-causal (KKR non-compliant) models that are widely used for approximating the permittivity of metals. A comparative analysis reveals a simultaneous increase in performance (as characterized by the error objective) and a reduction in the cardinality of the parameterization, often yielding more physically meaningful interpretations. These results are obtained without compromising model fidelity in regions of sharp Gaussian interband character, indicating that the proposed model provides an excellent alternative to previously proposed models.

OCIS codes: 160.3900, 160.2100, 310.6188, 310.6860, 310.6805

http://dx.doi.org/10.1364/ao.XX.XXXXXX

1. INTRODUCTION

The design and manufacture of optics and electronics depend on accurate knowledge of the optical properties of the materials involved [1, 2]. Commercial and industrial applications cover a wide range of precision-designed technologies, including: optoelectronics, thin films, optical interference devices (*e.g.*, mirrors, beam splitters, filters), sensing devices, fiber optics, and microelectronics (*e.g.*, integrated circuits) [1, 3–6]. The frequency domain representation of the polarization response of a material—or its *permittivity*—can be used to compute these properties. For this reason, closed form models are an indispensable theoretical tool for characterizing the optical properties of a given medium. Such expressions also present a convenient alternative to tabular data, providing a compact and continuous means for replicating experimental results. Furthermore, compatibility requirements of modern theoretical frameworks may necessitate closed form definitions [7–9].

Permittivity models are generally constructed by linearly superposing (in the frequency domain) individual functional descriptions of the various physical mechanisms underlying the macroscopically observed response. Harmonic oscillators commonly provide the appropriate basis for both the functional form and the physical interpretation of the response. However, the classical Drude-Lorentz theory is incapable of reproducing in detail the profiles empirically observed for many real materials unless additional, unphysical oscillators are added. To address this issue, a phenomenological approach is often adopted that seeks to formulate a more complete oscillator definition relative to the intended application. The scope of such an approach is often targeted at an entire class of materials [3, 10, 11].

The Brendel-Bormann (BB) oscillator is one such phenomenological definition [11]. It results from an approach that was originally proposed to capture the non-Lorentzian broadening observed in the infrared response of glasses [12]. This type of broadening typically has a profile somewhere between that of pure Lorentzian and a pure Gaussian. A number of classes of materials have been found to exhibit such behavior [3, 10, 11, 13, 14]. While the BB model is effective in reproducing these profiles, it has been recently shown that the model fails the Kramers-Kronig criteria for physical consistency of material response functions [15]. In Ref.[15] the authors have also proposed a novel model that produces the desired *tunable* Gaussian-Lorentzian profiles, while adhering strictly to the Kramers-Kronig relations. The proposed model is capable of accurately reproducing the broadened profiles observed in amorphous materials and glasses. In the present work, we show that a similar approach can also

be applied to the anomalous interband behavior that departs substantially from the classical profiles predicted by the Drude-Lorentz theory in some metals.

The organization of this work is as follows. In the remainder of this section, a brief discussion of linear optical response theory is presented within the context of the Kramers-Kronig formalism. In Sec. 2, the various model definitions are described and their features are discussed. A qualitative and parametric comparison between the classical profile and the non-Lorentzian profiles is also given. In Sec. 3, a reductive modeling procedure—motivated from both a dynamical and a mathematical viewpoint—is outlined for obtaining an optimal parameterization of a general model structure. The utility of the procedure is demonstrated in Sec. 4, where parameterizations are obtained for several real metals. The source data used here is identical to that used in the works of Rakić and collaborators. The source data include the optical properties of thin metallic films commonly used in the optoelectronic device industry [3]. The results of the present work are compared to [3]. An analysis of the results is given within the context of model performance, physical consistency, and physical interpretability.

A. The Linear Optical Response

The linear polarization P_i of a homogeneous material subject to a low intensity electromagnetic field E_i is given at a time t by the convolution [16]

$$P_i(t) = \int_{-\infty}^{\infty} G_{ij}(t-t')\,E_j(t')\,dt', \tag{1}$$

where G_{ij} is the Green's function tensor describing a general anisotropic material response. For isotropic and cubic media, the tensor relations are diagonal in all coordinate systems and scalar expressions may instead be used [17]. Then under a Fourier transform, one can relate the polarization to the displacement field to arrive at an expression for the relative permittivity of the medium:

$$\varepsilon = 1 + \chi, \tag{2}$$

where the electric susceptibility χ is the Fourier transform of the material response function G. Over absorptive bands, the permittivity becomes complex-valued (due to phase loss) and frequency-dependent. For conductive media, it is appropriate to decompose the corresponding complex susceptibility as

$$\chi(\omega) = \sum_{\phi}\chi_{\phi}(\omega) + \sum_{\beta}\chi_{\beta}(\omega), \tag{3}$$

where ϕ are the free electron (or intraband) absorptive mechanisms and β are the bound electron (or interband) absorptive mechanisms. The complex permittivity is related to the complex refractive index $\tilde{n} = n + i\,k$ by

$$\begin{aligned}\varepsilon &= \tilde{n}^2,\\ &= n^2 - k^2 + i\,2\,n\,k,\end{aligned} \tag{4}$$

so that the latter may always be computed if the former is known. Here n and k characterize the optical dispersion and absorption, respectively. In conjunction with Fresnel's well-known relations, the absorptive-dispersive indices represent a powerful means for obtaining many useful radiative and optical properties. Knowledge of these properties is critical to the application-specific material design required for, *e.g.*, optics and microelectronic device manufacture.

B. Kramers-Kronig Relations

A physically meaningful response function must obey the principle of relativistic causality. This means that a causal response is one resulting from an event strictly contained within its historical light cone. If one considers an impulsive field $E(t) = \delta(t)$ (where $\delta(t)$ is the Dirac delta function) incident on an isotropic medium, then the sifting property applied to (1) yields $P_\delta(t) = G(t)$. This implies that $G(t)$ is the (impulse) response at time t to the impulsive event at time $t = 0$. Accordingly, the principle of causality is such that a causal response function has the property $G(t) \equiv 0\,\forall\, t < 0$.

It has been established by Titchmarsh in [18] that this result is equivalent to the statement that the real and imaginary parts of the corresponding Fourier transform (*i.e.*, the susceptibility) form a Hilbert transform pair. If, in addition, the susceptibility is a Hermitian function—that is, if its inverse Fourier transform into the time domain is a real-valued function—then the Kramers-Kronig criteria are satisfied and the corresponding relations may be written for media with nonzero DC conductivity σ_0 [17]:

$$\begin{aligned}\chi'(\omega) &= \frac{2}{\pi}\,\mathcal{P}\int_0^{\infty}\frac{\overline{\omega}\,\chi''(\overline{\omega})}{\overline{\omega}^2-\omega^2}\,d\overline{\omega},\\ \chi''(\omega) &= \frac{4\,\pi\,\sigma_0}{\omega} - \frac{2}{\pi}\,\mathcal{P}\int_0^{\infty}\frac{\omega\,\chi'(\overline{\omega})}{\overline{\omega}^2-\omega^2}\,d\overline{\omega}.\end{aligned} \tag{5}$$

with $\chi' = \mathbb{R}\mathrm{e}\{\chi\} \in \mathbb{R}$ and $\chi'' = \mathbb{I}\mathrm{m}\{\chi\} \in \mathbb{R}$, and where $\mathcal{P}$ implies that the Cauchy principal value should be recovered from the singular, improper integral. The corresponding relations for non-conductive media are obtained by setting $\sigma_0 = 0$ in (5).

When obtained directly in the frequency domain, it is not readily apparent whether a given model corresponds to a real (*i.e.*, physically possible) material. The Kramers-Kronig relations are useful in this regard. To avoid the mathematical expense of verifying that the relations in (5) hold, one can instead leverage the assumptions introduced during their derivation [19, 20]:

1. $\chi(\omega)$ is analytic in the upper half complex plane,
2. $\chi(\omega) \to 0$ as $|\omega| \to \infty$ at least as fast as $1/|\omega|$, and
3. $\chi(\omega)$ is Hermitian.

The first condition implies that χ has no singularities in the upper half complex plane [21] and the third condition implies that $\chi(-\omega) = \chi^*(\omega)$, where χ^* is the complex conjugate of χ. If these conditions hold, then the susceptibility model satisfies the Kramers-Kronig criteria for physical consistency of a real material.

C. Important Note on Model Consistency

The adherence of a given model to the KKRs extends beyond simple frequency domain data point reproduction. Models violating the KKRs will generally produce spurious results when used in certain theoretical frameworks. One example is the Finite Difference Time Domain (FDTD) method applied to frequency dependent materials [22]. This method utilizes the time domain material response, which is the inverse Fourier transform of the model. A KKR-noncompliant model will generally produce an invalid time-domain response when inverted over absorptive bands.

2. MODELS

A. Classical Models

The classical interband absorption model has the form of a Complex Damped Harmonic Oscillator (CDHO) [23]:

$$\chi_k^L(\omega;\,\omega_k) \triangleq \frac{\omega_p^2\, f_k}{\omega_k^2 - \omega^2 - i\,\Gamma_k\,\omega}, \tag{6}$$

where the parameters are the oscillator strength f_k, the Lorentz broadening Γ_k, and the Lorentz resonance ω_k. The plasma frequency ω_p is a global material parameter.

The expression (6) is equivalent to the Fourier transform of a second order ordinary differential equation describing the harmonic motion of a periodically forced mass m having a restoring force κ with Lorentz resonance $\sqrt{\kappa/m}$. The Drude *free* electron model is then obtained by setting the corresponding restoring force to zero, leading to

$$\chi_k^D(\omega) \triangleq -\frac{\omega_p^2\, f_k}{\omega\,(\omega + i\,\Gamma_k)}. \tag{7}$$

Substitution of (6) and (7) into (2) and (3) yields the classical permittivity model.

The CDHO is sometimes found to be insufficient when modeling the interband absorption in metals since it is not capable of reproducing sharp transitions and therefore may over predict absorption in the profile wings [3, 23].

B. Brendel-Bormann Oscillator

In order to deal with excessive absorption in the wings of the classical interband model, Rakić *et al.* [3] have proposed that the CDHO be replaced with an expression defined in an earlier paper by Brendel and Bormann [11]. The expression is based on a convolution of the Gaussian profile and the Lorentzian profile. The convolution was originally introduced by Efimov and Khitrov to capture the broadened peaks observed in the infrared response of glasses [12]. The Efimov-Khitrov (EK) convolution is defined as

$$\chi_k^{EK}(\omega) \triangleq \int_{-\infty}^{\infty} \chi_k^G(\,y - \omega_k)\,\chi_k^L(\omega;\,y)\,dy, \tag{8}$$

where the Gaussian decay is

$$\chi_k^G(\,\omega_k) \triangleq \frac{1}{\sqrt{2\,\pi}\,\sigma_k}\exp\left[-\left(\frac{\omega_k}{\sqrt{2}\,\sigma_k}\right)^2\right], \tag{9}$$

with σ_k being the Gaussian broadening parameter. The EK convolution was evaluated by Brendel and Bormann as [3, 11]

$$\chi_k^{BB}(\omega) \triangleq \frac{i\,\omega_p^2\, f_k}{2\sqrt{2}\,\sigma_k\, a_k}\left[w\left(\frac{a_k - \omega_k}{\sqrt{2}\,\sigma_k}\right) + w\left(\frac{a_k + \omega_k}{\sqrt{2}\,\sigma_k}\right)\right], \tag{10}$$

under the condition that $\mathbb{I}\mathrm{m}\{a_k\} = \mathbb{I}\mathrm{m}\{\sqrt{\omega^2 - i\,\Gamma_k\,\omega}\} > 0$, where $w(z) \triangleq \exp(-z^2)\,\mathrm{erfc}(z)$ is the Faddeeva function with $\mathrm{erfc}(z)$ being the complex complimentary error function, and where $a_k = a_k' + i\,a_k''$ with

$$\begin{aligned} a_k' &\triangleq \frac{\omega}{\sqrt{2}}\{[1 + (\Gamma_k/\omega)^2]^{1/2} + 1\}^{1/2}, \\ a_k'' &\triangleq \frac{\omega}{\sqrt{2}}\{[1 + (\Gamma_k/\omega)^2]^{1/2} - 1\}^{1/2}, \end{aligned} \tag{11}$$

being defined such that $a_k'' > 0$. It has been shown in [15] that the BB model fails the Kramers-Kronig criteria in two respects: (1) it is not causal due to a singularity at the origin imposed by the a_k parameter in the denominator of the leading fractional term, and (2) it does not have a real-valued time domain expression (*i.e.*, inverse Fourier transform) since it lacks Hermicity. In other words, materials modeled with this oscillator violate well-known physical constraints and therefore are not found in nature.

C. Physically Consistent Gauss-Lorentz Oscillator

In [15], we derived an oscillator model that provides the same Gaussian broadening of a CDHO profile given by the BB model. This proposed new model also adheres strictly to the Kramers-Kronig criteria, and will henceforth be referred as the Gauss-Lorentz (GL) oscillator. The model is

$$\chi_k(\omega) \triangleq \mathcal{A}_k\,\mathcal{S}_k(\omega), \tag{12}$$

where $\mathcal{A}_k \triangleq \omega_p^2\, f_k/\omega_k^2$ is the amplitude at $\omega = 0$ and

$$\mathcal{S}_k(\omega) \triangleq \left(\frac{s_w(z_+) + s_w(z_-)}{\chi_0}\right), \tag{13}$$

is a dimensionless shape function with

$$\begin{aligned} s_w(z) &\triangleq i\,\pi\,w(z) \\ &\quad + \exp(-z^2)\left[\log(z) + \log\left(-\frac{z^*}{|z|^2}\right) - i\,\pi\right], \end{aligned} \tag{14}$$

where $\log(z)$ is the complex logarithm, z^* is the complex conjugate of z, $|z| = \sqrt{z\,z^*}$, and $z_\pm \triangleq (\pm\alpha_k - \omega_k)/\sqrt{2}\,\sigma_k$. Here $\alpha_k = \alpha_k' + i\,\alpha_k''$:

$$\begin{aligned} \alpha_k' &\triangleq (\omega/2)^{1/2}\,[(\omega^2 + \Gamma_k^2)^{1/2} + \omega\,]^{1/2}, \\ \alpha_k'' &\triangleq (\omega/2)^{1/2}\,[(\omega^2 + \Gamma_k^2)^{1/2} - \omega\,]^{1/2} + \mu, \end{aligned} \tag{15}$$

with μ being an arbitrary small constant ($0 < \mu << 1$). Note that the expressions in (11) are real-valued, whereas the expressions in (15) are generally complex-valued for $\omega < 0$. The shape function in (13) has been normalized by

$$\chi_0 \triangleq -4\,\sqrt{\pi}\,D\left(-\frac{\omega_k}{\sqrt{2}\,\sigma_k}\right), \tag{16}$$

where

$$D(x) \triangleq (\sqrt{\pi}/2)\exp(-x^2)\,\mathrm{erfi}(x), \tag{17}$$

is known as Dawson's function, which is related to the Faddeeva function: $D(x) = (\sqrt{\pi}/2)\,\mathbb{I}\mathrm{m}\{w(x)\}$, with $x \in \mathbb{R}$. Here, $\mathrm{erfi}(z) \triangleq -i\,\mathrm{erf}(i\,z)$ is the imaginary error function. The expression (16) has been defined so that $\mathcal{S}_k(\omega = 0) \equiv 1$. That is, the shape function has unity DC gain.

A comparison of the absorption profiles for the CDHO, the BB oscillator, and the proposed GL interband model is given Fig. 1. The figure demonstrates that the BB model and the GL model both produce the same 'tunable' Gaussian character, and that this differs from the Lorentzian profile of the CDHO by attenuation of absorption away from resonance. The benefit of the convolution type profile is that one can achieve either purely Lorentzian ($\sigma_k/\Gamma_k \to 0$) or purely Gaussian ($\Gamma_k/\sigma_k \to 0$) profiles, as well as any "interpolated" profile between the limiting cases.

An intended consequence of the definition proposed in (12) is the property $\chi_k(\omega = 0) = \chi_k^L(\omega = 0;\,\omega_l) = \mathcal{A}_k$. That is, the model is asymptotically equivalent to the CDHO. Furthermore, the energy absorption maximum of the proposed model has

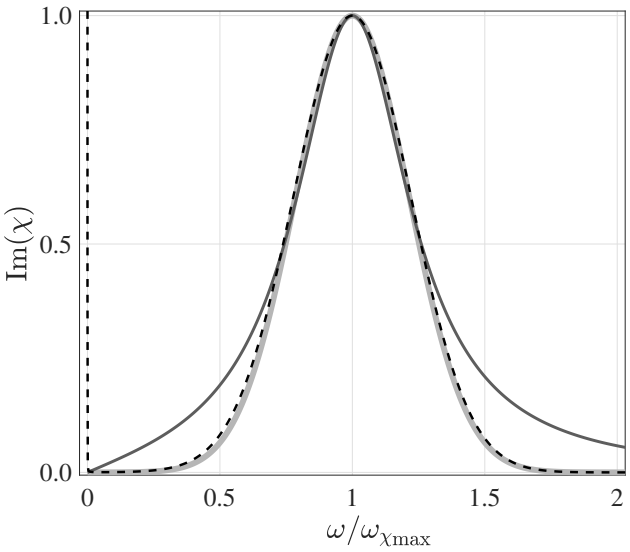

Fig. 1. Absorption profile shape comparison for the CDHO (solid dark), the BB oscillator (dashed), and the proposed interband model (solid light). The profile magnitudes have each been normalized and plotted on grids that are independently scaled by the spectral coordinates of the respective profile maxima (in order to align the profiles). The parameters are $\Gamma_k = k_\Gamma\,\omega_k$ and $\sigma_k = k_\sigma\,\omega_k$, with $k_\Gamma = \{0.510, 0, 0\}$ and $k_\sigma = \{\emptyset, 0.206, 0.214\}$ for the Lorentz, BB, and proposed models, respectively. With the profiles defined (and normalized) in this way, $\omega_p\,\sqrt{f_k}$ and ω_k can be arbitrarily chosen to yield the profiles above, with each having a full width at half maximum of 0.5. This demonstrates the invariant shape dependence of the profiles on the parameters Γ_k and σ_k. The sharp decay of the Gaussian profile clearly represents attenuated wing absorption. Note the divergence of the BB profile for $\omega \to 0$.

an energy coordinate, $E_{\max} = \hbar\,\omega_{\chi_{\max}}$, that is nearly identical to that of the corresponding CDHO. Both are approximately equal to $E_k = \hbar\,\omega_k$. This is preferable since it means that models expressed with the proposed configuration will tend toward agreement with empirically observed critical points. Then if the empirical observations agree with theoretical predictions, the model obtains some extent of parametric fidelity. These features are demonstrated in Fig. 2.

D. 3-Parameter Gaussian Oscillator

A Kramers-Kronig consistent 3-parameter complex (pure) Gaussian oscillator may be obtained from the previously noted model by setting $\Gamma_k = 0$. That is, by replacing α_k defined in (15) with $\overline{\alpha}_k = \overline{\alpha}'_k + i\,\overline{\alpha}''_k$:

$$\begin{aligned}\overline{\alpha}'_k &\triangleq (\omega/2)^{1/2}\,(|\omega| + \omega)^{1/2},\\ \overline{\alpha}''_k &\triangleq (\omega/2)^{1/2}\,(|\omega| - \omega)^{1/2} + \mu.\end{aligned} \tag{18}$$

This is useful result because it allows the more general model to converge all the way to the Gaussian limit. This provides a means for model reduction as described further on.

3. IMPLEMENTATION

Since the fidelity of a given model structure is realized through the specific parameterization, we give attention here not only to the proposed model, but also to the manner in which the parameterizations were obtained. The importance of such details should not be overlooked, since the procedure involves minimizing an objective function that is highly nonlinear in the model parameters. This implies that the fidelity of a given model is coupled to the user's experience with mathematical optimization. We qualify this statement in a later assessment of models obtained for real materials, which are generated from experimental data identical to that used in the work of Rakić *et al.* in [3].

The efforts of Rakić and collaborators provide an appropriate reference for a comparative analysis of modeling fidelity. This is because their work provides a comprehensive survey of the efficacy of the BB model when modeling interband absorption effects for a number of metals relevant to the manufacture of optoelectronic devices. For each of the 11 metals considered, they also provide a comparison to the classical Drude-Lorentz theory. Their models were obtained by relying fundamentally on their proprietary global optimization algorithm [24, 25]. We take a similar approach with respect to the novel physically consistent oscillator. Here, however, we utilize a more systematic reductive method that considers each oscillator separately (rather than surveying a single type over the entire model bandwidth). This method utilizes nonlinear programming initialized from the global result to achieve the results, as described presently.

Over the course of obtaining the parameterizations given in the present work, a simple-yet-effective procedure was developed for systematically improving the model fits described in [3]. This improvement was obtained for both the classical Drude-Lorentz parameterizations and for those given in terms of the proposed GL interband oscillators. In each case, the performance improvement can be characterized qualitatively, in terms of the point wise error residuals, especially in the interband regions near the upper bound of the model bandwidth. The performance improvement can also be characterized quantitatively, in terms of the objective function defined in [3]:

$$\mathcal{V}_c(\theta) \triangleq \sum_{m=1}^{M} [|\Delta_r(\omega_m;\,\theta)| + |\Delta_i(\omega_m;\,\theta)|]^2, \tag{19}$$

with

$$\begin{aligned}\Delta_r(\omega_m;\,\theta) &\triangleq [\varepsilon'(\omega_m;\,\theta) - \varepsilon'_m]/\varepsilon'_m,\\ \Delta_i(\omega_m;\,\theta) &\triangleq [\varepsilon''(\omega_m;\,\theta) - \varepsilon''_m]/\varepsilon''_m,\end{aligned} \tag{20}$$

and where $\varepsilon(\omega;\,\theta) = \varepsilon'(\omega;\,\theta) + i\,\varepsilon''(\omega;\,\theta)$ is the respective model evaluated at a frequency ω given a parameter set θ. Here $\varepsilon_m = \varepsilon'_m + i\,\varepsilon''_m$ is the experimental data defined on an M-sized frequency grid, ω_m, $m \in [1, M]$. The subscript c in (19) denotes the consideration of error dynamics which are coupled (or dependent) with respect to the model. This is represented by the existence of cross terms in (19).

A. General Procedure

The proposed procedure is based on addressing the existence of features in the real and imaginary parts of the data that may be uncoupled (or independent) with respect to the model. An example of such a feature is related to the nonlocal spatiotemporal field dependence known as the anomalous skin effect [26]. The traditional treatment for this effect in bulk materials is necessary when the mean free path of the conduction electrons is on the order of the field penetration depth (known as the 'skin depth') [27–29]. For thin films of the monovalent noble metals, the skin depth may be on the order of the sample thickness. In these

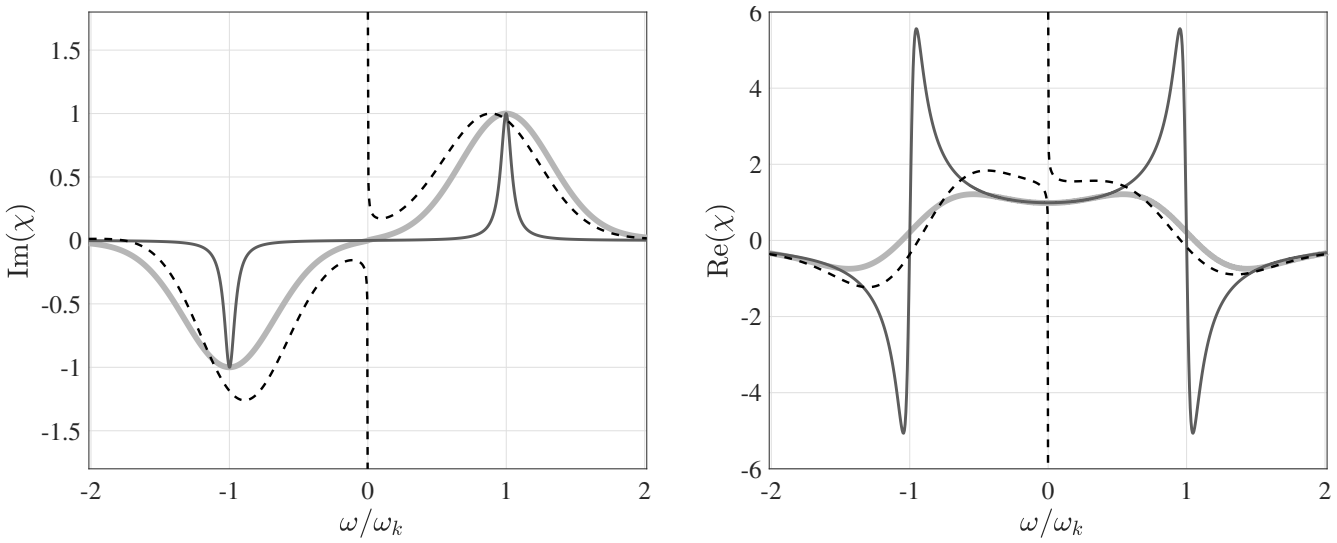

Fig. 2. Comparison with CDHO: imaginary (left plot) and real (right plot) parts of the CDHO (thin dark gray line), the BB oscillator (dashed black line), and the proposed oscillator (thick light gray line). The parameters are: $\omega_p\sqrt{f_k} = 9.01\sqrt{0.050} = 2.015$, $\Gamma_k = 0.189$, $\omega_k = 2.025$, and $\sigma_k = 0.631$. The units are eV with f_k dimensionless. The parameters have been taken directly from the $k = 1$ oscillator used in the silver model given in [3] where σ_k has been decreased by a factor of 3 for the purposes of visual clarity (the noted undesirable effects are enhanced at greater σ_k). The imaginary part of each model has been normalized in the right half plane. The proposed model is asymptotically equivalent to the CDHO at $\omega = 0$ and for $\omega \to \pm\infty$. Furthermore, the energy absorption maxima for the proposed model and the CDHO are approximately equal, with both occurring at approximately ω_k (*i.e.*, when $\omega/\omega_k = 1$). Figure adapted from [15] with permission.

films it has be shown that the anomalous skin effect, which manifests at room temperatures, can be expressed as a decoupled correction in the (purely imaginary) loss function with respect to the classical Drude analysis [30] at higher energies. Other examples include the frequency dependent damping resulting from carrier-carrier interaction [31] (which is apparent a lower energies), and multiple scattering mechanisms found in metallic compounds [32] or due to surface impurities [33].

Features such as these may depart in an systematically and independent way from mismatch in the defined model space over a given band. In order to account for these kinds of errors, it is logical to perform a secondary minimization over an objective where independent mismatch is considered. For this purpose, we define auxiliary objective function:

$$\mathcal{V}_u(\theta) \triangleq \sum_{m=1}^{M} \Big\{ [\psi_r(\omega_m)\,|\Delta_r(\omega_m;\,\theta)|]^2 + [\psi_i(\omega_m)\,|\Delta_i(\omega_m;\,\theta)|]^2 \Big\}, \tag{21}$$

where the subscript u denotes the fact that the mismatch terms are uncoupled. The frequency-dependent weighting functions ψ_r and ψ_i can be used to emphasize relevant energetic regimes, and to suppress undesirable effects imposed by implicit grid weighting or by systematic model mismatch occurring over the several orders of magnitude typically traversed by the permittivity of conductive media (*i.e.*, over the intraband region). In order to more completely address implicit grid effects (and thereby improve system conditioning), we have also preconditioned the grid in accordance with the findings of Pintelon and Kollár in [34].

As a rule, the weighting functions should be designed in accordance with the demands placed on the model by the intended application. For example, to mitigate the effects due to the intraband region, one may take

$$\psi_r(\omega_m) = \psi_i(\omega_m) = |\omega_m^p|, \tag{22}$$

where p can be used to emphasize ($p > 0$) or de-emphasize ($p < 0$) dynamics as a function of frequency. In many cases, a simple uncoupling without grid weighting (*i.e.*, $p = 0$) is sufficient. For data with more complicated intraband dynamics, we found $p = 1/4$ to be a reasonable value for improving the fit at higher frequencies. This can and should be adjusted as needed on a case-by-case basis to improve fitting of the interband region, but without neglecting lower frequencies. To localize the emphasis (or de-emphasis) to specific features or regions—such as, *e.g.*, fast Gaussian transitions—one may define the weightings

$$\psi_r(\omega_m) = \psi_i(\omega_m) = \psi_f^{-|\hbar\omega_m - E_f|}, \tag{23}$$

where $\psi_f \in \mathbb{R} > 0$ determines the magnitude of the emphasis ($\psi_f > 1$) or de-emphasis ($0 < \psi_f < 1$), and E_f is the photon energy about which the relevant feature is centered. We found this useful in attending to transitions at the absorption edge of, *e.g.*, the monovalent noble metals.

The models were initialized from the parameterizations given in [3]. At each step requiring objective minimization, nonlinear programming was employed [35]. Many off-the-shelf software packages exist for this type of non-convex minimization, such as MATLAB's *fmincon*. The entire procedure, outlined in the flowchart of Fig. 3, can be grouped into three sections: (a) procedure initialization, (b) main fitting loop, and (c) finalization criteria. As indicated in the flowchart, the fundamental benefit is obtained (as previously noted) by successively minimizing the uncoupled and coupled error objectives defined in (21) and

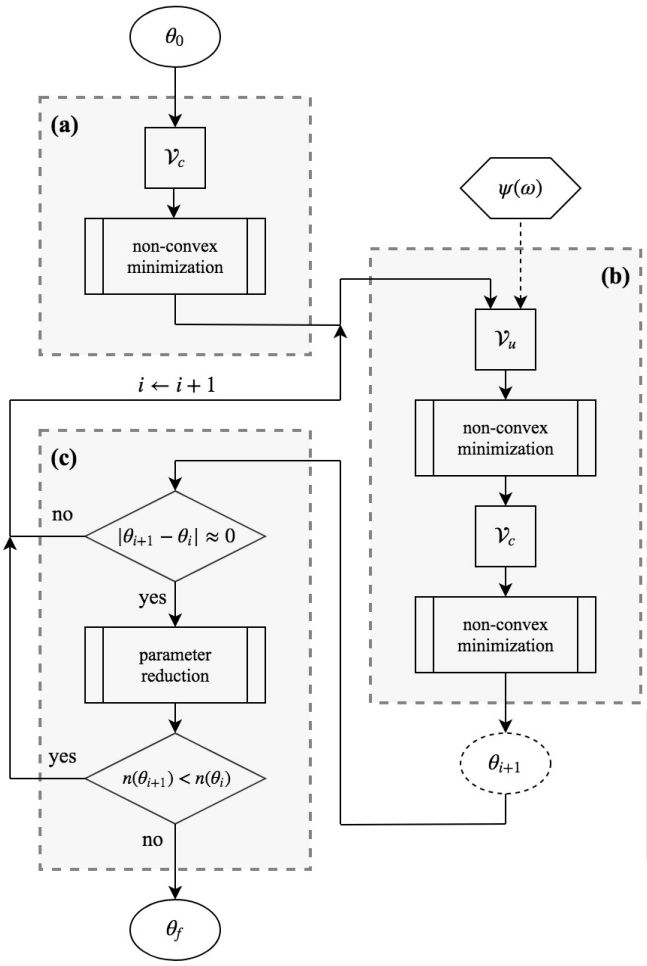

Fig. 3. Fitting procedure: (a) initialization, (b) main fitting step, and (c) finalization. The sections (b) and (c) constitute an iterative loop. The initial set θ_0 is obtained via a global algorithm such as that given in [24, 25]. The weightings $\psi(\omega)$, if defined, are used only with $\mathcal{V}_u$ as defined in (21). The finalization step (c) is exited if there is no significant change in the parameters between two consecutive iterations and if the model complexity is not reduced. The final model is given by θ_f.

(19), respectively. The weightings, if defined, are only used on an interim basis and play no role in assessing the fidelity of the resulting model. All results shown in the following section are given in terms of the objective function (19) originally defined in [3].

B. Reductive Modeling

In order to arrive in a more consistent manner at a conclusive assessment of the efficacy of a given model structure (*e.g.*, Gaussian, Lorentzian, or Gauss-Lorentz), we employ a reductive technique that involves beginning with the more general structure of (12). Once refined, the model can be used to infer the usefulness a particular oscillator configuration.

As discussed in [15], the second term of $s_w(z)$ in (14) may misbehave, producing very large values if $\sigma_k/\Gamma_k \to \beta_k$ (for some small value β_k) due to the exponential term. This is related to enforcement of the Hermitian requirement of the Kramers-Kronig relations. When this occurs, it implies that the GL oscillator should be replaced with a simple CDHO. Thus, the appropriate strategy for fitting the GL type oscillator is to temporarily replace $s_w(z)$ in (13) with $\widetilde{s}_w(z) \triangleq i\,\pi\,w(z)$ during minimization, thereby omitting the Hermitian correction term of (14). This is useful since these terms will tend to interfere during the main portion minimization process and they can be easily reinstated after the CDHO reduction is applied. Once the temporarily modified model structure has been fit, the full form of (14) is reinstated and any resulting oscillators that misbehave as previously described are replaced with the CDHO of (6).

Whenever $\Gamma_k/\sigma_k \to 0$, the GL oscillator achieves a purely Gaussian profile equivalent in shape to that described in [10] and is replaced with the 3-parameter model previously discussed.

If after fitting a model, one finds that a particular oscillator contributes negligibly to the model (*i.e.*, $f_k \approx 0$), then that oscillator should be removed entirely. See, for example, the Titanium model given in Tbl. 3 of [3], where $f_4 = 0.0002$.

Another possibility for reducing the model complexity is related to the description of "two-electron" type behaviors in the intraband region. This happens when a CDHO can be replaced with a Drude term. This is discussed in more detail in the results section.

If any of the aforementioned model reductions has been applied, the main step of the fitting procedure is once again applied. This is indicated by the iteration loop between sections (b) and (c) in the flowchart of Fig. 3.

C. Efficient Computation of Dispersion Integrals

Evaluation of the various error function types and dispersion integrals is a demanding task, both in terms of efficiency and in terms of accuracy. For these purposes, we suggest the excellent suite of functions written by Johnson [36], which have been implemented in C++ and have wrappers for most common computing syntaxes (*e.g.*, MATLAB, Python, R, and Julia). The reader is cautioned against evaluating the Faddeeva and Dawson functions by directly compositing the functions, as this may produce results with unacceptable accuracy.

4. RESULTS AND DISCUSSION

When discussing the models obtained in [3], we will refer to the Reference Brendel-Bormann (RBB) model or to the Reference Drude-Lorentz (RDL) model. We refer to the Proposed Gauss-Lorentz (PGL) model, the Proposed Drude-Lorentz (PDL) model, or to the Proposed Composite (PC) model when referencing those from the present work. The PC designation implies that combinations of the proposed Gauss-Lorentz oscillators and the classical oscillators are used.

An important note that should be clarified is that the novel GL type model structure and the fidelity of the models obtained using the fitting procedure are not dependent on one another. The benefit of the novel GL model, discussed in [15], is that it adheres strictly to the KKRs. As noted previously, this means that models utilizing the proposed GL oscillator are suitable for use beyond simple data point reproduction. They can be used in generalized simulation frameworks that require KKR consistency in order to produce meaningful results (*e.g.*, the FDTD method [22]). This will not generally be the case for models which do not adhere to the KKRs, such as the BB model. These motivations are further supported by the fact that KKR analysis is often an integral part of the data gathering process. It stands to reason then that models obtained on this data should also observe the KKRs.

A. Silver (Ag)

The data for silver were compiled from three sources, all of which are tabulated and described in detail in [37]. The first two sources primarily define the intraband region, while the latter is mainly representative of interband behaviors. The ellipsometric data of Dold and Mecke [38] are used for 0.125–0.980 eV. Over the range 0.650–3.300 eV, the data of Winsemius *et al.* [39]—which are also the result of ellipsometric measurements—are used, leading to a region of overlap in the data from 0.650–0.980 eV where there is some disagreement in the values for ε''. Over the interband region 3.40–6.00 eV, the data of Leveque *et al.* [40] are used. These were obtained by Kramers-Kronig analysis/transform methods applied to combined direct *in situ* reflectance measurements and curve extrapolation supported by reflectance values derived (indirectly) from other sources.

The experimental data is plotted alongside the RBB model and the PC model in Fig. 4. It should be noted that recent measurements for both Ag and Au [41, 42] have shown that the measurements of $|-\varepsilon'|$ given by Dold and Mecke are spuriously low, and are, in fact, not Kramers-Kronig consistent [43]. This accounts for the systematic disagreement between the experimental data in the region of overlap, and also suggests a reason for the poor model fit in this region. The sharp interband transition representing a departure from a purely Lorentzian profile can be observed in ε'' around 4 eV. The RBB model obtains the objective value $\mathcal{V}_c = 3793.55$ in 22 parameters with 1 intraband term and 5 interband terms (of the BB type). The PC model represents a significant improvement, with $\mathcal{V}_c = 8.04$ obtained in just 14 parameters with 1 intraband term and 4 interband terms (1 of the CDHO type and 3 of the 3-parameter GL type). The model parameters are given in Tbl. 1. The gray entry in the table denotes a parameter that can be removed without affecting the model fidelity (as described in a later section), leading to a 13 parameter model. One observes that in [3], the experimental data noted above was used to fit the model, but the authors of that work chose to plot only the range 0.125–5.00 eV, omitting from their plot the last 1 eV of bandwidth. In Fig. 4, we have plotted the entire modeled bandwidth.

B. Gold (Au)

The ellipsometric data of Dold and Mecke [38] were used for the portion of the intraband region on the range 0.125–0.980 eV. In [31], Thèye gives an excellent comprehensive analysis of the optical properties of Au, verifying empirically the analyses with spectrophotometric reflectance and transmittance measurements of semitransparent Au films. This data is used for the range 1.000–6.000 eV, which covers the remainder of the intraband region and the onset of the interband region. Both of the aforementioned sets are conveniently tabulated in [37].

The RBB model and the PGL model are plotted alongside the experimental data in Fig. 5. As previously discussed, the data of Dold and Mecke for $|-\varepsilon'|$ are spuriously low-valued (see discussion for silver). The non-Lorentzian transition is observed in ε'' around 2 eV. The RBB model obtains the objective value $\mathcal{V}_c = 8204.45$ in 22 parameters with 1 intraband term and 5 interband terms (of the BB type). The PGL represents a significant reduction in model mismatch, with $\mathcal{V}_c = 3.45$ obtained in 14 parameters with 1 intraband term and 4 interband terms (1 of the CDHO type and 3 of the 3-parameter GL type). The model parameters are given in Tbl. 1. The gray entry in the table denotes a parameter that can be removed without affecting the model fidelity (as described in a later section), leading to a 13 parameter model. In [3], the experimental data noted above was used to fit the model, but the authors of that work chose to plot only the range 0.200–5.000 eV. In Fig. 5, we have plotted the entire modeled bandwidth.

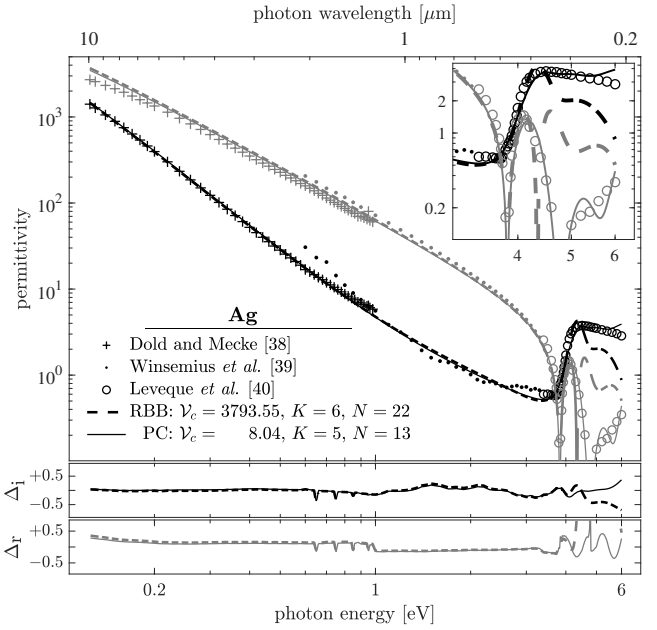

Fig. 4. Permittivity of silver: $|-\varepsilon'|$ (gray) and ε'' (black) given in terms of experimental data (markers) and models (lines). K denotes the number of oscillators and N denotes the number of parameters, as given in Tbl. 1. The residual subplots are in terms of (20).

C. Copper (Cu)

Data for copper was obtained from the study of Ordal *et al.* [44], where reflectance measurements were combined with Kramers-Kronig analysis/transform methods to obtain the dispersive-absorptive optical indices. A similar procedure was followed by Hagemann *et al.* [45], who applied Kramers-Kronig analysis/transform methods to transmittance measurements to obtain the complex optical index. The data of Ordal *et al.* was used for the greater portion of the intraband range 0.093–0.867 eV and the data of Hagemann *et al.* were used on the range 1.000-6.000 eV which describes the remainder of the intraband behaviors as well as the interband region. The composite set can be found tabulated in [37].

The RBB model and the PGL model are plotted alongside the experimental data in Fig. 6. The sharp Gaussian transition in ε'' is observed near 2 eV. The RBB model yields the objective minimum $\mathcal{V}_c = 2.75$ in 18 parameters with 1 intraband term and 4 interband terms (of the BB type). The PGL produces an objective minimum of $\mathcal{V}_c = 1.80$ obtained in 14 parameters with 1 intraband term and 4 interband terms (1 of the CDHO type and 3 of the 3-parameter GL type). The model parameters can be found in Tbl. 1. As in the cases of both Ag and Au, the gray entry in the table denotes a parameter that can be removed without affecting the model fidelity (as described in a later section), leading to a 13 parameter model.

D. Aluminum (Al)

In [46], Rakić combined several sources of data for evaporated aluminum films along with application of the Kramers-Kronig

Table 1. Model Parameters and Objective Minima

θ	Ag	Au	Cu	Al	Be	Cr	Ni	Pd	Pt	Ti	W
$\omega_p^\dagger$	9.01	9.03	10.83	14.98	18.51	10.75	15.92	9.72	9.59	7.29	13.22
f_0^*	0.790	0.718	0.517	0.401	0.080	0.176	0.094	0.347	0.324	0.143	0.202
Γ_0	0.053	0.046	0.024	0.041	0.033	0.051	0.033	0.011	0.078	0.078	0.057
f_1^*	0.382	0.109	0.128	0.349	0.087	0.392	0.423	0.905	0.244	0.303	0.014
Γ_1	22.952	0.439	0.370	0.239	1.892	2.214	2.964	7.242	0.602	0.612	
ω_1	0.187	0.162	0.053	0.009	0.268	0.712	0.763	0.474	0.814	0.356	0.971
σ_1								0.612		0.231	0.149
f_2^*	0.033	0.045	0.091	0.082	0.681	0.999	0.173	0.271	1.251	0.257	0.593
Γ_2				0.418	2.765	2.466	2.206	1.033	3.632	1.024	1.296
ω_2	4.341	2.828	2.842	1.572	2.653	1.990	4.690	0.560	1.721	1.149	1.882
σ_2	0.238	0.345	0.532		1.094						0.785
f_3^*	0.074	0.265	0.398	0.165	0.085	0.489	0.663	0.022	3.427	0.707	0.057
Γ_3				1.849			1.764		10.592		
ω_3	4.814	3.834	4.809	1.997	4.793	7.440	10.973	1.587	9.158	1.987	3.456
σ_3	0.411	0.811	1.126		0.706	0.997		15.978		0.991	0.342
f_4^*	0.459	1.453	0.785								1.622
Γ_4											1.212
ω_4	6.284	6.966	8.869								5.693
σ_4	0.948	1.907	1.357								1.100
$\mathcal{V}_c(\theta)$	8.04	3.45	1.80	0.92	0.47	2.92	0.21	0.62	0.87	1.23	1.59

†Fixed during optimization. *Dimensionless. All others in eV. Blank σ_k entries denote CDHO configurations. Blank Γ_k entries denote 3-parameter (complex) Gaussian configurations. Gray entries denote removable parameters (by Drude substitution).

formalism and a proprietary iterative algorithm to arrive at a single, physically consistent data set covering the intra- and interband regions over the range 0.006–15.100 eV.

As indicated in Tbl. 1, Aluminum is one of three models for which the fitting method selected the classical model (the other two are Ni and Pt). The RDL model returns an objective value of $\mathcal{V}_c = 1.04$ in 14 parameters with 1 intraband term and 4 interband terms (of the CDHO type). The PDL obtains a minimum of $\mathcal{V}_c = 0.92$ in 11 parameters utilizing 1 intraband term and 3 interband terms (of the CDHO type). The models and data are plotted in Fig. 7. The model cardinality is further reduced by removing the gray colored entry in Tbl. 1, leading to a 10 parameter model that retains the noted objective value. The transitions marked by $\hbar\omega_2 = 1.572$ eV and $\hbar\omega_3 = 1.997$ eV are supported by band theoretical calculations [47], as well as by the empirical fits of, *e.g.*, [46].

E. Beryllium (Be)

The beryllium data covering the range 0.020–5.000 eV are taken entirely from the work of Arakawa *et al.* [48], who performed extensive conditioning on several sets of reflectance measurement data. Subsequent application of Kramers-Kronig analysis/transform methods provided the complex refractive index.

The RDL model obtains a relatively low objective minimum of $\mathcal{V}_c = 0.63$ using a total of 14 parameters in 1 intraband term and 4 interband terms (of the CDHO type). The PC model obtains a value of $\mathcal{V}_c = 0.47$ in 12 parameters with 1 intraband term and 3 interband terms (1 of the CDHO type, 1 of the 4-paramter GL type, and 1 of the 3-paramter GL type). The model parameters are given in Tbl. 1. The gray entry in the table denotes a parameter that can be removed without affecting the model fidelity, leading to an 11 parameter model. We found that the inclusion of the Gaussian broadened oscillators was necessary in order to reduce the number of interband oscillators, as using 3 CDHO oscillators was found to be insufficient for accurately modeling dynamics in the interband region. Furthermore, the interband excitation parameters $\hbar\omega_2 = 2.653$ and $\hbar\omega_3 = 4.793$ are in approximate agreement with the empirical and band theoretical values reported in the literature [49, 50] (which would not be the case if the GL type oscillators had been omitted). The data and models are plotted in Fig. 8.

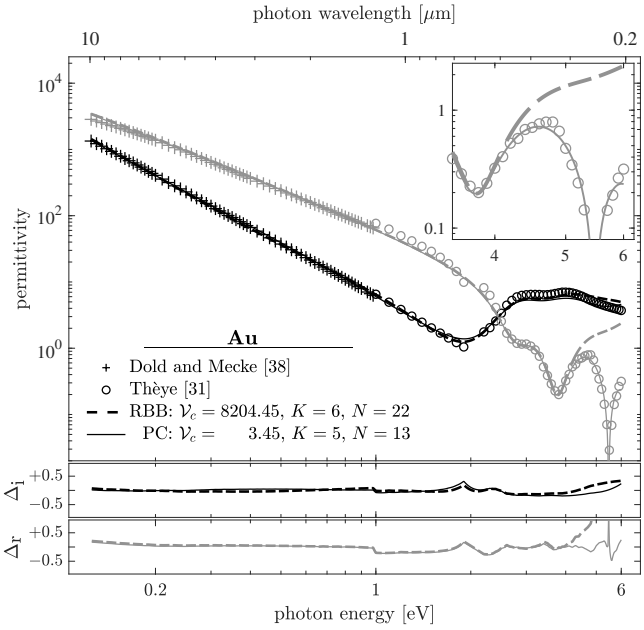

Fig. 5. The same as Fig. 4, except for gold.

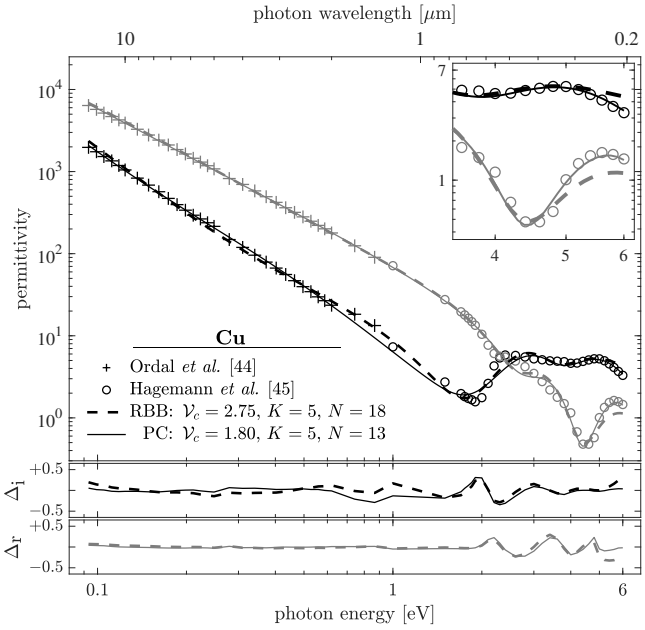

Fig. 6. The same as Fig. 4, except for copper.

F. Chromium (Cr)

The greater portion of the intraband region covering 0.069–0.413 eV for the chromium models was provided by the study of Kirillova and Noskov [51]. Their measurements in this region were obtained by infrared spectrometric measurements. Data for the remainder of the intraband region extending into the interband region was provided by the works of Bos and Lynch [52] for the range 0.460–5.000 eV. Their analysis included measurements of the absorptivity (rather than the reflectivity) in order to better distinguish the subtle character of the interband region [52].

The RDL model yields an objective minimum of $\mathcal{V}_c = 2.97$, obtaining this value in 14 parameters with 1 intraband term and 4 interband terms (of the CDHO type). The PC model obtains a minimum of $\mathcal{V}_c = 2.92$ in 11 parameters with 1 intraband term and 3 interband terms (1 of the 3-parameter GL type and 2 of the CDHO type). The parameter set is given in Tbl. 1 corresponding the models plotted in Fig. 9. The values inside the model bandwidth $\hbar\omega_1 = 0.712$ eV and $\hbar\omega_2 = 1.990$ eV find approximate agreement with band calculations obtained for higher energy transitions in [52].

G. Nickel (Ni)

The studies of Lynch *et al.* [53] and of Vehse and Arakawa [54] provide data for nickel, which was obtained by application of Kramers-Kronig analysis/transform methods to absorptivity and reflectance measurements, respectively. Data from [53] were used for the intraband region 0.200-3.000 eV, while data from [54] was used for modeling the interband regime covering 3.100–5.000 eV. These data were combined and tabulated in [37], which is the reference given in [3].

The modeling results for nickel are perhaps the most conclusive in determining the utility of the proposed fitting procedure. It is the second of three materials for which the fitting procedure selected an entirely classical model (the other two being Al and Pt). The RDL model provided in [3] yields the objective value $\mathcal{V}_c = 3.42$ in 14 parameters utilizing 1 intraband term and 4 interband terms (of the CDHO type). The PDL model obtains the minimum $\mathcal{V}_c = 0.21$ in 11 parameters with the use of 1 intraband term and only 3 interband terms (of the CDHO type). Qualitatively, one observes that the PDL model provides a much more accurate representation of both ε' and ε'' in the interband region of Fig. 10. There is also a mismatch in the RDL model of ε'' in the low energy regime that is resolved by the PDL model.

The PDL model values $\hbar\omega_1 = 0.763$ eV and $\hbar\omega_2 = 4.690$ eV agree with values reported in the literature [53–56] for interband transitions. Band calculations in [55, 57] predict a broadened structure centered near 0.80 eV representing weak electronic transitions. As in the case of beryllium, a meaningful reduction in the cardinality of the parameterization yields a significant reduction in model mismatch while also providing a more physically interpretable model.

H. Palladium (Pd)

The study of Weaver and Benbow [58] provides the data for the range 0.100–0.600 eV, extending just past the peak occurring near 0.4 eV. They obtained their data using absorptivity measurements obtained by a calorimetric technique which was then paired with Kramers-Kronig analysis to obtain the phase shift. The optical constants were then computed directly. Data obtained from reflection and transmission measurements on the range 0.640–6.000 eV by Johnson and Christy [56] were used for the remainder. The tabulated data for both studies can be found in [59].

The best minimum from [3] is given by the RDL model, which obtains $\mathcal{V}_c = 6.35$ in 14 parameters using 1 intraband term with 4 interband terms (of the CDHO type). The PC model represents a significant improvements, returning $\mathcal{V}_c = 0.62$ in 12 parameters with 1 intraband term and only 3 interband terms (1 of the 4-parameter GL type, 1 of the 3-parameter GL type, and 1 of the CDHO type). In [3], the author's have plotted the initial portion of the experimental fit up to 5 eV. In Fig. 11, we have plotted the entire experimental range. Band theory predicts low energy interband structure at ≈ 5 eV [60], which

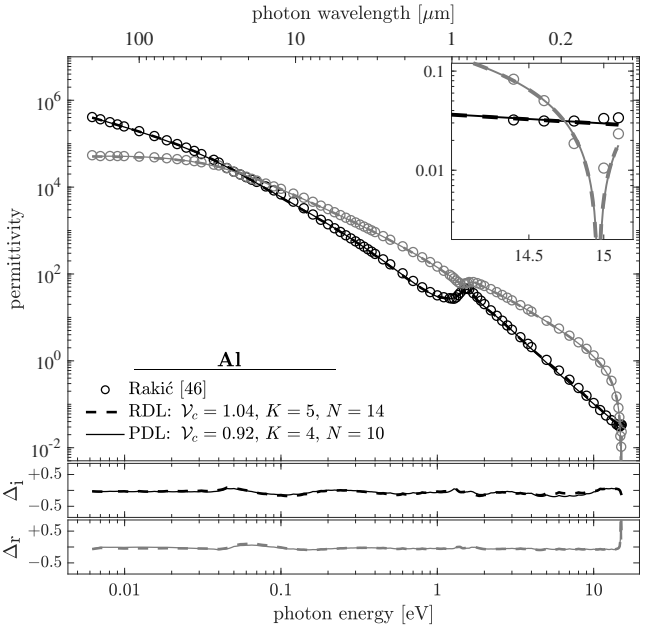

Fig. 7. The same as Fig. 4, except for aluminum.

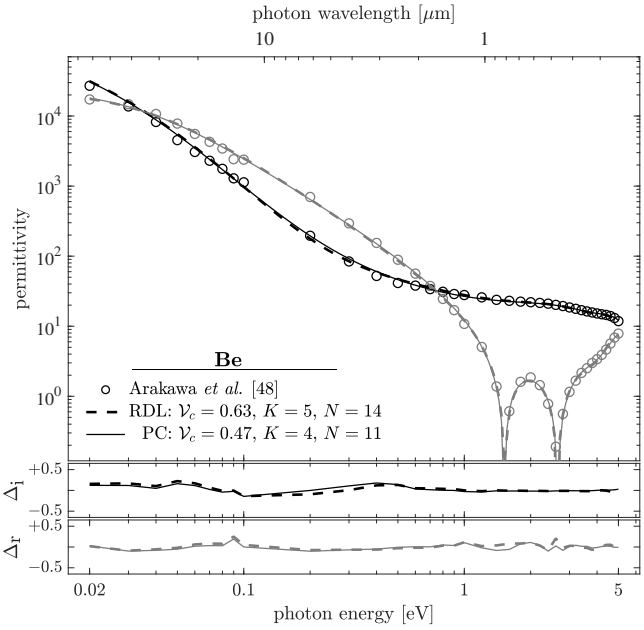

Fig. 8. The same as Fig. 4, except for beryllium.

is confirmed by the empirical findings of multiple authors [58]. This likely corresponds to both $\hbar\omega_1 = 0.474$ eV and $\hbar\omega_2 = 0.560$ parameters, which jointly define this region.

I. Platinum (Pt)

In [61], Weaver applies Kramers-Kronig analysis on Drude-like data extrapolation of his own reflectance measurements into the infrared regime in order to obtain a continuous permittivity data set below 4 eV. He combined this with data from a number of other sources to extend the range to higher values. The experimental data used here is the range 0.100–5.000 eV.

Platinum is the third of three materials for which the modeling procedure selected a purely classical model (the former two being Al and Ni). The data and models are plotted in Fig. 12. The RDL model is given in 14 parameters with 1 intraband term and 4 interband terms (of the CDHO type), yielding an objective minimum of $\mathcal{V}_c = 0.86$. The PDL model yields a nearly equivalent minimum of $\mathcal{V}_c = 0.87$, but does so in only 11 parameters expressed in 1 intraband term and 3 interband terms (of the CDHO type). The parameters for our model are provided in Tbl. 1. As noted in [61], both d-like and p-like transitions can be found in the band structure of platinum that correspond to the resonance parameter $\hbar\omega_2 = 0.814$ eV. The value $\hbar\omega_2 = 1.721$ eV is likely unphysical, providing support to the other portions of the obtained model. Interestingly, the value $\hbar\omega_3 = 9.158$ eV resulting from the minimization—which falls well outside the modeled range—is near the value 9.5 eV predicted by band calculations that has also been observed empirically at around 9.8 eV [61].

J. Titanium (Ti)

Separate studies conducted by Kirillova and Charikov have provided data for both the intraband [62] and interband [63] regions, respectively. We have modeled the same range selected in [3]: 0.062–2.610 eV. Measurements for the latter of the two studies were obtained from ellipsometric measurements, while those from the former were obtained by spectrometric measurements extending into the infrared regime.

The minimum obtained by the RBB model is $\mathcal{V}_c = 1.38$, which is achieved in 18 parameters corresponding to 1 intraband term and 4 interband terms (of the BB type). A nominal improvement in the objective is obtained by the PC model with $\mathcal{V}_c = 1.23$, but with a significant reduction in the cardinality of the parameterization. Only 12 parameters are required, with 1 intraband term and 3 interband terms (1 of the 4-parameter GL type, 1 of the 3-parameter GL type, and 1 of the CDHO type). The models and data are plotted in Fig. 13 with the corresponding parameters given in Tbl. 1.

K. Tungsten (W)

The data for tungsten taken from Weaver *et al.* [64] are also tabulated in [37]. These cover the range 0.100–5.000 eV. Weaver and collaborators obtained absorptivity and reflectivity measurements on polished crystalline samples. Calorimetry was used to obtain absorptivity measurements for the initial range up to 4.4 eV with reflectivity measurements from synchrotron radiation making up the remainder. Permittivity was then obtained using Kramer-Kronig analysis with supplementary data sources aiding in high-energy extrapolation.

The RBB model consists of 18 parameters with 1 intraband term and 4 interband terms (of the BB type), and obtains an objective minimum of $\mathcal{V}_c = 10.42$. The PGL model requires just 16 parameters with 1 intraband term and 4 interband terms (2 of the 4-parameter GL type and two of the 3-parameter GL type) to achieve a minimum of $\mathcal{V}_c = 1.59$. The parameters are provided in Tbl. 1 and the results are plotted in Fig. 14. Each of the resonant parameters obtained by the PGL model corresponds to directly to absorptivity maxima noted by Weaver and coworkers in [64].

L. Model Analysis

One should note a subtle-yet-important trend in the parameterizations of Tbl. 1. Many of the $k = 1$ oscillators have the property

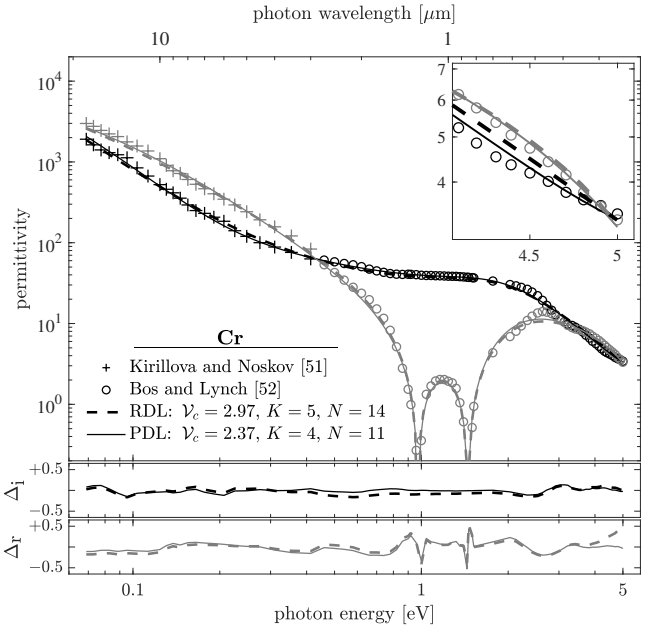

Fig. 9. The same as Fig. 4, except for chromium.

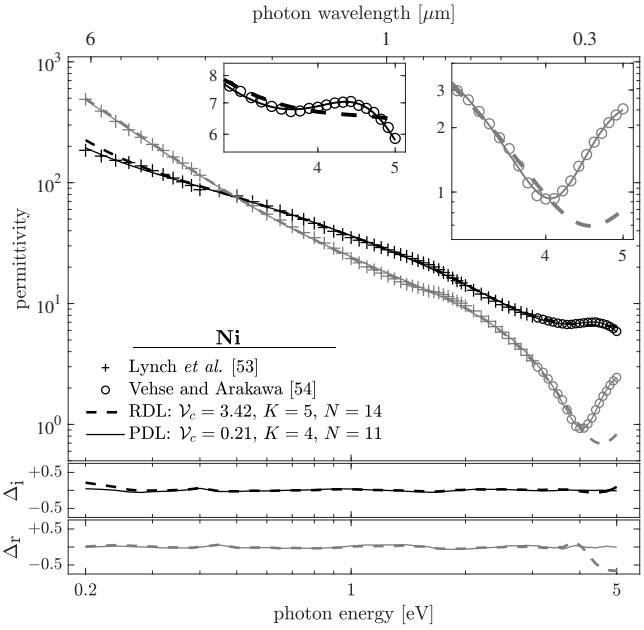

Fig. 10. The same as Fig. 4, except for nickel.

$\Gamma_1 >> \omega_1$, whereas for the $k > 1$ oscillators the reverse is often true. The former is not generally a meaningful parameter assignment for the time constants of bound electrons. A closer inspection reveals that these terms are approximating a secondary Drude-like process (in the intraband region). In some cases, the multiple Drude-like terms correspond to features such as the (previously noted) anomalous skin effect and electron-electron interactions [30]. The emergence of these terms by optimization supports the Drude-Roberts two-electron theory [65], with the auxiliary Drude-like term in Ag being related to surface impurities and the type observed in Au being related to the previously noted considerations [33].

To expand upon this point, we consider the $k = 0$ and $k = 1$ terms from the Au model, which we will designate as the primary and auxiliary Drude terms, respectively. The low energy roll-off of the auxiliary term causes the model to effectively transition regimes having differing time constant dependencies. To show this, we consider the extended Drude analysis [41, 66], whereby a frequency-dependent time constant, $\tau(\omega)$, is derived according to

$$\frac{1}{\tau(\omega)} = \frac{\omega\,\varepsilon''(\omega)}{\varepsilon_\infty - \varepsilon'(\omega)}. \tag{24}$$

The high frequency contribution, ε_∞, is estimated by fitting the expression

$$\varepsilon(\omega) = \varepsilon_\infty - \frac{\omega_p^2}{\omega^2 + i\,\omega\,\Gamma}, \tag{25}$$

over a limited energy range. By fitting the experimental data up to 3 eV, we obtain for our estimate $\varepsilon_\infty \approx 5.3$. As noted in [41], the analysis is relatively insensitive to errors in this estimation, which become negligible in the low frequency limit where our analysis takes place. The results of this analysis are plotted in Fig. 15.

The figure demonstrates three important details: (1) the auxiliary Drude term facilitates a transition corresponding to the frequency dependence of the mean free path time constant for an extended Drude theory; (2) the (inverse) time constant transitions from the classical theory at higher energies to the quadratic regime predicted by the Fermi liquid theory (for electron-electron interactions), but then continues on to a dependence which has a logarithmic grid dependence at lower energies; and (3) both the subtle and the prominent features found in the data of Dold and Mecke [38] are consistent with recent findings [41, 42]. The more recent study has shown that at energies below 0.1 eV, the time constant has an exponential frequency dependence. These features were found to exist outside of experimental uncertainty.

For Ag, Au, Cu, Al, and Be, one can safely replace the $k = 1$ CDHO with a simple Drude oscillator using the given $\{f_1, \Gamma_1\}$ pairings and without affecting the model fidelity (qualitatively or quantitatively), thereby reducing the parameterization in those cases by 1. This is indicated by the gray entries in Tbl. 1. There is no need to plot these modifications, since they yield precisely the same results previously demonstrated in Figures 4 through 8. In the case of Cr, Ni, and Pd, the additional Drude-like CDHO terms cannot be reduced to a simple Drude term, since the dependence on the entire CDHO is more substantial, being related, as previously noted, to the effects of lower energy transitions.

The models obtained for Be, Cr, Pd, Ti, and W—whose parametric reduction was found to be dependent on the use of GL type oscillators—suggest that the conclusions of [3] (*i.e.*, that Gauss-Lorentz type oscillators are primarily useful for in Au, Ag, and Cu) may not be entirely accurate, since most of the models in that study were evidently over parameterized, so that the additional degrees of freedom in those models may tend to mask the utility of the Gaussian type oscillators beyond the noted cases. Regardless, the resulting parameterizations of the present study suggest two regimes of behavior in the noble metals Ag, Au, and Cu. Specifically, the intraband regime is subject to dynamics which are more completely described by multiple Drude-like terms, whereas the interband regime obtains its best

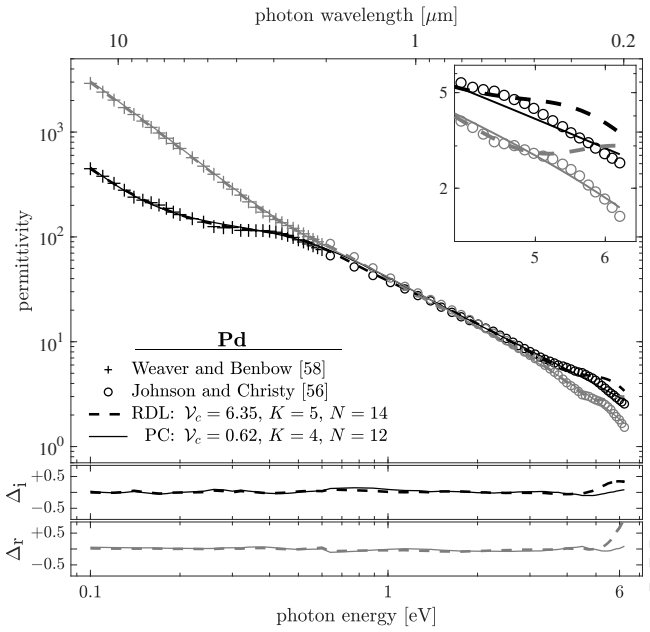

Fig. 11. The same as Fig. 4, except for palladium.

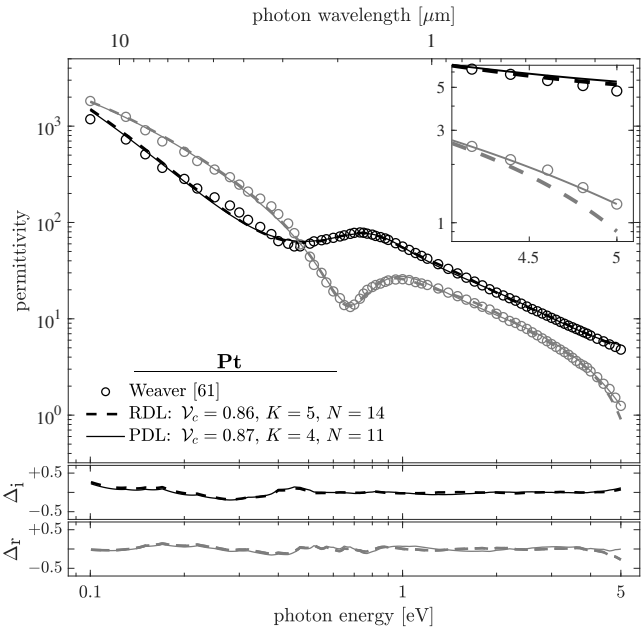

Fig. 12. The same as Fig. 4, except for platinum.

parametric minimum in a *purely* Gaussian description.

5. CONCLUSIONS

The optical properties of a given medium result from its polarization response to electromagnetic forcing. In the frequency domain, models for this response often take the form of a linear combination of harmonic oscillators representing the various mechanisms underlying the absorption profile over a given energetic bandwidth. In order for a given model to generally represent a real (*i.e.*, physically possible) material, it must adhere to a set of physical constraints known as the Kramers-Kronig Relations (KKRs). These KKRs ensure that a model can be used in generalized simulation frameworks.

The Brendel-Bormann (BB) oscillator has often been used to capture the Gaussian character observed in the absorption profiles of real materials. However, the BB oscillator does not satisfy the KKRs. Models based on BB oscillators do not generally represent real materials and may produce spurious results when used in certain simulation frameworks. Recently, a model has been proposed that accurately reproduces this Gaussian character while also adhering strictly to the KKRs [15].

Here we extend the range of utility for the model proposed in [15] to the interband character of metals (notably the sharp transitions observed in Ag, Au, and Cu). A detailed and generic procedure is given for finding an optimal parameterization of the intraband-interband response in terms of the physically consistent model. The procedure, when combined with the general model structure, allows for a reductive modeling approach. The resulting optimized models represent a significant qualitative and quantitative improvement over those obtained in previous studies utilizing KKR-noncompliant BB oscillators to achieve the same purpose.

The models obtained using the proposed procedure with the novel KKR-compliant oscillator simultaneously reduce the model mismatch and the number of parameters needed for high accuracy. This implies a reduction in unphysical overfitting and improvement in fidelity. The results demonstrate the utility of the procedure and indicate that properly parameterized models tend to reveal the more accurate and reduced nature of the model components while also improving the physical interpretability of the model.

REFERENCES

1. D. Franta, D. Nečas, and I. Ohlídal, "Universal dispersion model for characterization of optical thin films over a wide spectral range: application to hafnia," Appl. Opt. **54**, 9108–9119 (2015).
2. G. E. Jellison, Jr. and F. A. Modine, "Parameterization of the optical functions of amorphous materials in the interband region," Appl. Phys. Lett. **69**, 371–373 (1996).
3. A. D. Rakić, A. B. Djurišić, J. M. Elazar, and M. L. Majewski, "Optical properties of metallic films for vertical-cavity optoelectronic devices," Appl. Opt. **37**, 5271–5283 (1998).
4. J. Kischkat, S. Peters, B. Gruska, M. Semtsiv, M. Chashnikova, M. Klinkmüller, O. Fedosenko, S. Machulik, A. Aleksandrova, G. Monastyrskyi, Y. Flores, and W. T. Masselink, "Mid-infrared optical properties of thin films of aluminum oxide, titanium dioxide, silicon dioxide, aluminum nitride, and silicon nitride," Appl. Opt. **51**, 6789–6798 (2012).
5. C. C. Kim, J. W. Garland, H. Abad, and P. M. Raccah, "Modeling the optical dielectric function of semiconductors: Extension of the critical-point parabolic-band approximation," Phys. Rev. B **45**, 11749–11767 (1992).
6. D. J. Goldie, A. V. Velichko, D. M. Glowacka, and S. Withington, "Ultra-low-noise MoCu transition edge sensors for space applications," J. Appl. Phys. **109**, 084507–1–084507–9 (2011).
7. A. Vial and T. Laroche, "Description of dispersion properties of metals by means of the critical points model and application to the study of resonant structures using the FDTD method," J. Phys. D Appl. Phys. **40**, 7152–7158 (2007).
8. E. A. Muljarov and W. Langbein, "Resonant-state expansion of dispersive open optical systems: Creating gold from sand," Phys. Rev. B **93**, 075417–1–075417–6 (2016).
9. H. S. Sehmi, W. Langbein, and E. A. Muljarov, "Optimizing the Drude-Lorentz model for material permittivity: Method, program, and exam-

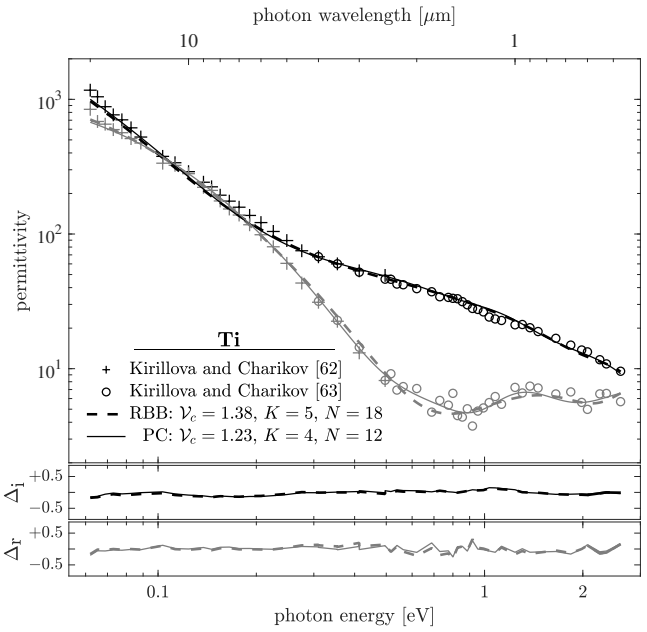

Fig. 13. The same as Fig. 4, except for titanium.

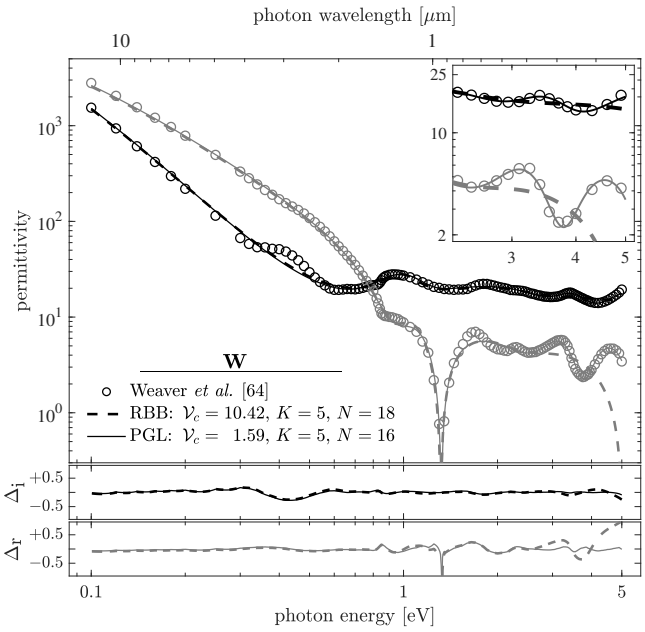

Fig. 14. The same as Fig. 4, except for tungsten.

ples for gold, silver, and copper," Phys. Rev. B **95**, 115444–1–115444–8 (2017).
10. A. D. Rakić and M. L. Majewski, "Modeling the optical dielectric function of GaAs and AlAs: Extension of Adachi's model," J. Appl. Phys. **80**, 5909–5914 (1996).
11. R. Brendel and D. Bormann, "An infrared dielectric function model for amorphous solids," J. Appl. Phys. **71**, 1–6 (1992).
12. A. M. Efimov, "Quantitative IR spectroscopy: Applications to studying glass structure and properties," J. Non-Cryst. Solids **203**, 1–11 (1996).
13. D. D. S. Meneses, M. Malki, and P. Echegut, "Structure and lattice dynamics of binary lead silicate glasses investigated by infrared spectroscopy," J. Non-Cryst. Solids **352**, 769–776 (2006).
14. R. Kitamura, L. Pilon, and M. Jonasz, "Optical constants of silica glass from extreme ultraviolet to far infrared at near room temperature," Appl. Opt. **46**, 8118–8133 (2007).
15. J. Orosco and C. F. M. Coimbra, "Optical response of thin amorphous films to infrared radiation," Phys. Rev. B (2018).
16. F. Wooten, *Optical Properties of Solids* (Academic Press, New York, 1972).
17. V. Lucarini, K.-E. Peiponen, J. J. Saarinen, and E. M. Vartiainen, *Kramers-Kronig Relations in Optical Materials Research* (Springer, Berlin, Heidelberg, 2005).
18. E. C. Titchmarsh, *Introduction to the Theory of Fourier Integrals* (Oxford: Clarendon Press, 1962), 2nd ed.
19. R. de L. Kronig, "On the Theory of Dispersion of X-Rays," J. Opt. Soc. Am. **12**, 547–557 (1926).
20. H. A. Kramers, "La diffusion de la lumière par les atomes," in "Atti del Congresso Internazionale dei Fisici," , vol. 2 (N. Zanichelli, Bologna, 1927), vol. 2, pp. 545–557.
21. S. Lang, *Complex Analysis* (Springer, New York, 1999), 4th ed.
22. K. S. Kunz and R. J. Luebbers, *The Finite Difference Time Domain Method for Electromagnetics* (CRC Press, New York, 1993).
23. M. Q. Brewster, *Thermal Radiative Transfer & Properties* (Wiley, 1992).
24. A. D. Rakić, J. M. Elazar, and A. B. Djurišić, "Acceptance-probability-controlled simulated annealing: A method for modeling the optical constants of solids," Phys. Rev. E **52**, 6862–6867 (1995).
25. A. B. Djurišić, A. D. Rakić, and J. M. Elazar, "Modeling the optical constants of solids using acceptance-probability-controlled simulated annealing with an adaptive move generation procedure," Phys. Rev. E **55**, 4797–4803 (1997).
26. P. W. Gilberd, "The anomalous skin effect and the optical properties of metals," J. Phys. F Met. Phys. **12**, 1845–1860 (1982).
27. G. E. H. Reuter and E. H. Sondheimer, "The theory of the anomalous skin effect in metals," P. Roy. Soc. Lond. A Mat. **195**, 336–364 (1948).
28. R. B. Dingle, "The anomalous skin effect and the reflectivity of metals I," Physica. **19**, 311–347 (1953).
29. R. B. Dingle, "The anomalous skin effect and the reflectivity of metals: II. comparison between theoretical and experimental optical properties," Physica. **19**, 348–364 (1953).
30. M.-L. Thèye, "Anomalous skin effect and size effect in thin metallic films," Phys. Lett. A **25**, 764–765 (1967).
31. M.-L. Thèye, "Investigation of the Optical Properties of Au by Means of Thin Semitransparent Films," Phys. Rev. B **2**, 3060–3078 (1970).
32. J. W. Allen and J. C. Mikkelsen, "Optical properties of CrSb, MnSb, NiSb, and NiAs," Phys. Rev. B **15**, 2952–2960 (1977).
33. S. Roberts, "Interpretation of the Optical Properties of Metal Surfaces," Phys. Rev. **100**, 1667–1671 (1955).
34. R. Pintelon and I. Kollár, "On the Frequency Scaling in Continuous-Time Modeling," IEEE T. Instrum. Meas. **54**, 318–321 (2005).
35. J. Nocedal and S. J. Wright, *Numerical Optimization*, Springer Series in Operations Research (Springer, 2006), 2nd ed.
36. S. G. Johnson, "Faddeeva Package," http://ab-initio.mit.edu/wiki/index.php/Faddeeva_Package (2015).
37. D. W. Lynch and W. R. Hunter, "Comments on the optical constants of metals and an introduction to the data for several metals," in "Handbook of Optical Constants of Solids," E. D. Palik, ed. (Academic Press, Burlington, 1997), pp. 275–367.
38. B. Dold and R. Mecke, "Optische Eigenschaften von Edelmetallen, Übergangsmetallen und deren Legierungen im Infrarot (1. Teil)," Optik. **22**, 435–446 (1965).
39. P. Winsemius, H. P. Lengkeek, and F. F. V. Kampen, "Structure dependence of the optical properties of Cu, Ag and Au," Phys. B+C **79**, 529–546 (1975).
40. G. Leveque, C. G. Olson, and D. W. Lynch, "Reflectance spectra and dielectric functions for Ag in the region of interband transitions," Phys. Rev. B **27**, 4654–4660 (1983).
41. H. U. Yang, J. D'Archangel, M. L. Sundheimer, E. Tucker, G. D. Boreman, and M. B. Raschke, "Optical dielectric function of silver," Phys. Rev. B **91**, 235137–1–235137–11 (2015).
42. R. L. Olmon, B. Slovick, T. W. Johnson, D. Shelton, S.-H. Oh, G. D.

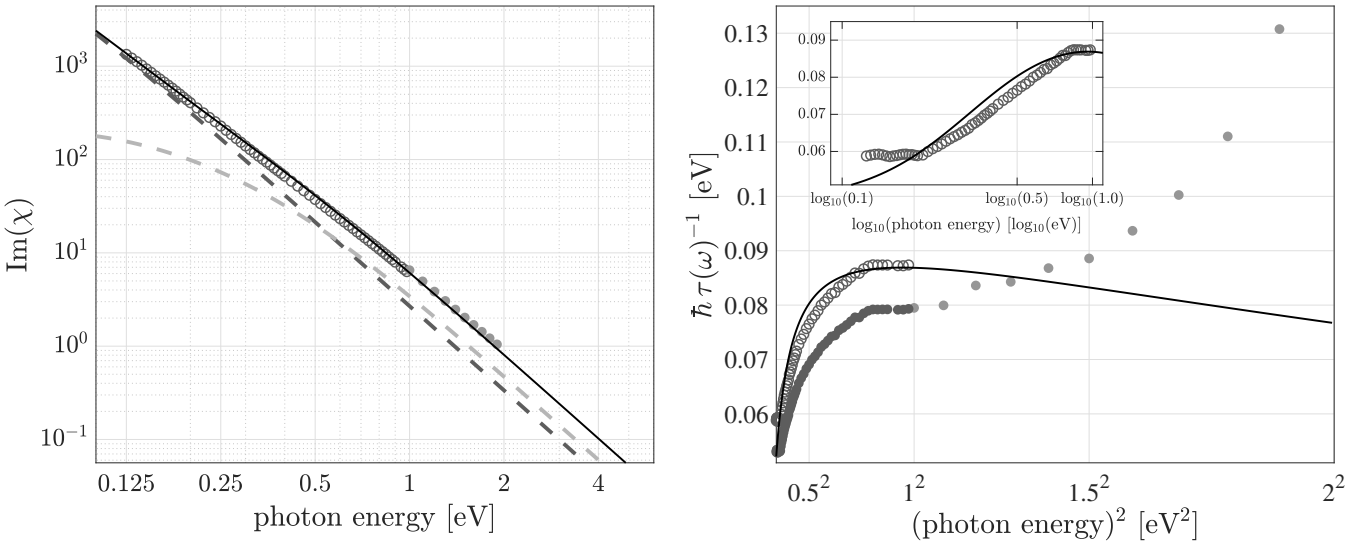

Fig. 15. Effect of multiple Drude-like terms on the intraband model of Au. Left plot: imaginary part of the primary $k = 0$ (thick, black, dashed) and secondary $k = 1$ (thick, gray, dashed) Drude terms from the Au model as listed in Tbl. 1. Right plot: inverse time constant. In each plot: the sum of the two Drude terms (thin, black, solid), the intraband data of Dolde and Mecke [38] (open circles), and the interband data of Thèye [31] (light gray dots). The dark gray dots in the right plot are the Dolde and Mecke data with the real part scaled by a factor of 1.11. This was done to more clearly demonstrate the continuous transition between regimes. The approximately linear region from about 1^2–1.5^2 eV^2 in the right plot represents the quadratic frequency dependence predicted by Fermi liquid theory. Higher energies clearly have a lower order dependence. The inset of the right plot displays the data below 1 eV on a logarithmically scaled grid, which demonstrates that the inverse time constant is proportional to the log-scaled grid over this band. The effect of the auxiliary Drude term is to allow the model to approximately reproduce this behavior. This effect is equivalent to the Drude-Roberts two-electron model [33, 65].

Boreman, and M. B. Raschke, "Optical dielectric function of gold," Phys. Rev. B **86**, 235147–1–235147–9 (2012).

43. H. U. Yang, J. D'Archangel, M. L. Sundheimer, E. Tucker, G. D. Boreman, and M. B. Raschke, "Supplemental material," (2015).
44. M. A. Ordal, R. J. Bell, R. W. Alexander, L. L. Long, and M. R. Querry, "Optical properties of fourteen metals in the infrared and far infrared: Al, Co, Cu, Au, Fe, Pb, Mo, Ni, Pd, Pt, Ag, Ti, V, and W." Appl. Opt. **24**, 4493–4499 (1985).
45. H.-J. Hagemann, W. Gudat, and C. Kunz, "Optical constants from the far infrared to the x-ray region: Mg, Al, Cu, Ag, Au, Bi, C, and Al_2O_3," J. Opt. Soc. Am. **65**, 742–744 (1975).
46. A. D. Rakić, "Algorithm for the determination of intrinsic optical constants of metal films: application to aluminum," Appl. Opt. **34**, 4755–4767 (1995).
47. H. Ehrenreich, H. R. Philipp, and B. Segall, "Optical properties of aluminum," Phys. Rev. **132**, 1918–1928 (1963).
48. E. Arakawa, T. Callcott, and Y.-C. Chang, "Beryllium (Be)," in "Handbook of Optical Constants of Solids," E. D. Palik, ed. (Academic Press, Burlington, 1997), pp. 421–433.
49. L. H. Jenkins, D. M. Zehner, and M. Chung, "Characteristic energy gain and loss, double ionization, and ionization loss events in Be and BeO secondary electron spectra," Surf. Sci. **38**, 327–340 (1973).
50. T. L. Loucks and P. H. Cutler, "Band structure and fermi surface of beryllium," Phys. Rev. **133**, A819–A829 (1964).
51. M. M. Kirillova and M. M. Noskov, "Optical properties of chromium," Phys. Met. Met. **26**, 189–192 (1968).
52. L. W. Bos and D. W. Lynch, "Optical properties of antiferromagnetic chromium and dilute cr-mn and cr-re alloys," Phys. Rev. B **2**, 4567–4577 (1970).
53. D. Lynch, R. Rosei, and J. Weaver, "Infrared and visible optical properties of single crystal Ni at 4 K," Solid State Commun. **9**, 2195–2199 (1971).
54. R. C. Vehse and E. T. Arakawa, "Optical and Photoemissive Properties of Nickel in the Vacuum-Ultraviolet Spectral Region," Phys. Rev. **180**, 695–700 (1969).
55. B. Cooper and H. Ehrenreich, "The ferromagnetic kerr effect in nickel," Solid State Commun. **2**, 171–174 (1964).
56. P. B. Johnson and R. W. Christy, "Optical constants of transition metals: Ti, v, cr, mn, fe, co, ni, and pd," Phys. Rev. B **9**, 5056–5070 (1974).
57. J. C. Phillips, "Fermi surface of ferromagnetic nickel," Phys. Rev. **133**, A1020–A1028 (1964).
58. J. H. Weaver and R. L. Benbow, "Low-energy interband absorption in pd," Phys. Rev. B **12**, 3509–3510 (1975).
59. A. Borghesi and A. Piaggi, "Palladium (Pd)," in "Handbook of Optical Constants of Solids," E. D. Palik, ed. (Academic Press, Burlington, 1997), pp. 469–476.
60. S. N. Rashkeev, Y. A. Uspenskii, and I. I. Mazin, "Optical properties of transition metals at infrared frequencies," Sov. Phys. **61** (1985).
61. J. H. Weaver, "Optical properties of rh, pd, ir, and pt," Phys. Rev. B **11**, 1416–1425 (1975).
62. M. M. Kirillova and B. A. Charikov, "Study of the optical properties of transition metals," Opt. Spectrosc. **17**, 134–135 (1964).
63. M. M. Kirillova and B. A. Charikov, "Optical properties of titanium in the quantum transition range," Phys. Met. Met. **15**, 138–139 (1963).
64. J. H. Weaver, C. G. Olson, and D. W. Lynch, "Optical properties of crystalline tungsten," Phys. Rev. B **12**, 1293–1297 (1975).
65. D. K. Edwards and N. Bayard De Volo, "Useful Approximations for the Spectral and Total Emissivity of Smooth Bare Metals," in "Advances in Thermophysical Properties at Extreme Temperatures and Pressures," S. Gratch, ed. (ASME, New York, 1965).
66. S. J. Youn, T. H. Rho, B. I. Min, and K. S. Kim, "Extended drude model analysis of noble metals," Phys. Status Solidi B **244**, 1354–1362 (2007).